

Influence of the Bulkiness of the Substituent on the Aggregation and Magnetic Properties of Poly(3-alkylthiophene)s

Helmuth Peeters,¹ Mihaela Jivanescu,² André Stesmans,² Lino M. C. Pereira,³ Leander Dillemans,⁴ Jean-Pierre Locquet,⁴ Margriet J. Van Bael,⁴ André Persoons,⁵ Guy Koeckelberghs¹

¹Laboratory for Polymer Synthesis, KU Leuven, Celestijnenlaan 200F, 3001 Heverlee, Belgium

²Semiconductor Physics Laboratory, KU Leuven, Celestijnenlaan 200D, 3001 Leuven, Belgium

³Nuclear and Radiation Physics Section, KU Leuven, Celestijnenlaan 200D, 3001 Leuven, Belgium

⁴Laboratory of Solid State Physics and Magnetism, KU Leuven, Celestijnenlaan 200D, 3001 Leuven, Belgium

⁵Laboratory of Molecular Electronics and Photonics, KU Leuven, Celestijnenlaan 200D, 3001 Heverlee, Belgium

Correspondence to: G. Koeckelberghs (E-mail: guy.koeckelberghs@chem.kuleuven.be)

Received 12 June 2013; accepted 4 October 2013; published online 29 October 2013

DOI: 10.1002/pola.26973

ABSTRACT: A series of poly(3-alkylthiophene)s (P3ATs) (P1–P5) has been synthesized via a Ni(dppp)-mediated polymerization, varying the bulkiness of the alkyl side chains in order to investigate the influence of the bulkiness of the alkyl substituent on the aggregation and magnetic properties of P3ATs. UV–Vis spectroscopy, performed in solution as well as in film, shows that the stacking of the polymers becomes more complicated as the bulkiness of the side chains increases. Both the π -interactions and the planarization of the polymer chains are diminished. While aggregation is absent in poor solvent for the polymer with the most bulky side chains, aggregation was present in film, albeit slowed down. This behavior was also confirmed by X-ray diffraction (XRD) and differential scanning

calorimetry (DSC) experiments. Electron spin resonance (ESR) measurements, performed at 300 K on powders, confirmed the trend of decreasing supramolecular order with increasing bulkiness of the side-chain. Magnetization measurements, performed at 5 and 300 K, are in line with our hypothesis on the influence of π -interactions and the fraction of planar polymer chains on the coercivity and saturation magnetization, respectively. © 2013 Wiley Periodicals, Inc. *J. Polym. Sci., Part A: Polym. Chem.* **2014**, *52*, 76–86

KEYWORDS: conjugated polymers; ESR; π -interactions; poly(3-alkylthiophene); magnetism; SQUID

INTRODUCTION Conjugated polymers have been explored intensively for many years. Their optical, electrical, and electronic properties¹ have been studied in detail, which has resulted in many applications, such as solar cells and light-emitting diodes. In contrast, the magnetic behavior has received far less attention. The main reason is that ferromagnetism in organic compounds requires the presence of unpaired electrons (spins) and that spins in organic molecules are typically paired. Nevertheless, unpaired spins can be present in organic molecules, in which case they are often introduced as radicals, carbenes, or by oxidation.^{2–4} A second requirement is a pathway by which unpaired spins interact (spin coupling).⁵ Within one molecule a conjugated π -system is ideal to act as a (ferro)magnetic linker between different spins. When stacked, there may also be inter-polymer (molecule) interaction between occurring spins. Therefore, conjugated polymers are in fact particularly suited as organic material possibly exhibiting (ferro)magnetic behavior. The

substitution pattern and the connectivity are crucial parameters for a (ferro)magnetic spin coupling causing spin alignment.⁶ Quite some “high-spin” molecules,^{7,8} oligomers,⁹ and polymers^{10–13} have been reported based on this approach and remarkable progress has been achieved.

Besides the “high-spin” molecules, also some conjugated polymers were reported as showing magnetic behavior under very specific conditions. Typical examples are poly(aniline)s,^{14–17} poly(pyrrole),¹⁸ regio-irregular poly(3-alkylthiophene)s (P3ATs),^{19–23} and (substituted) poly(acetylene)s.²⁴ In all these cases, the materials were chemically or electrochemically doped, introducing spins (polarons). In contrast to these results, we have previously reported on the magnetic behavior of *neutral* (undoped) poly(thiophene)s carrying an alkyl, alkoxy, or alkylthio sidechain.^{25,26} The samples were examined by ESR spectroscopy and SQUID magnetometry. The measurements reveal the presence of (at least) two

Additional Supporting Information may be found in the online version of this article.

© 2013 Wiley Periodicals, Inc.

spin systems. A first electron spin system gives rise to a paramagnetic behavior. A second spin system results in a ferromagnetic behavior with zero coercivity and remanence at 300 K and (for most polymers) with significant coercivity and remanence at 5 K. The origin of the latter spin system is unknown, but different from the ESR-active one. Although the origin of the spin systems and the way they interact is not fully understood, some hypotheses can nevertheless be made. First, the amount of Bohr-magneton measured by SQUID magnetometry seems to be dependent on the number of planar polymer chains. This might suggest that conjugation within one polymer chain is important. Second, concerning the coercivity, it was found that polymers in which strong π -interactions between stacked polymer chains are present show the highest coercivity. Therefore, it can be hypothesized that these π -interactions determine the ferromagnetic behavior (coercivity).

In this article, these hypotheses are tested by investigating a series of P3ATs (Fig. 1). P3ATs were preferred since they can be prepared using a controlled chain-growth mechanism^{27,28} providing optimal control on the molecular structure. Moreover, driven by π -interactions, P3ATs with linear side-chains have a strong tendency to stack. The polymers studied are all regio-regular (head-to-tail coupled) and have the same molar mass, but differ in the bulkiness of the substituent. In particular, a hexyl substituent was used in all cases, but an increasingly longer branched side chain was employed. The increase of the bulkiness should result in a larger distance between the stacked P3ATs, weakening the π -interactions, but leaving all other parameters unchanged. This should therefore allow the verification of the influence of π -interactions on coercivity. Moreover, in cases where the π -stacking is prevented by a bulky alkyl substituent, it might also affect the planarization of the polymer chains. These polymers thus not only allow the study of the influence of the π -interactions on the coercivity, but also the influence of the fraction of planar polymer chains on the number of Bohr magnetons.

Therefore, a first part of this article investigates how the bulkiness of the alkyl substituent influences the aggregation behavior of P3AT. Next, the magnetic properties of the polymers are studied and the aforementioned hypotheses are tested.

EXPERIMENTAL

Gel permeation chromatography (GPC) measurements were done with a Shimadzu 10A apparatus with a tunable absorbance detector and a differential refractometer in tetrahydrofuran (THF) as eluent toward polystyrene standards.

UV-vis spectra were recorded with a Varian Cary 400. The DSC experiments were performed on a DSC 7 from Perkin Elmer.

Films were prepared by spin coating from chloroform solutions (1 mg/0.1 mL) on a glass substrate (spinning speed: 1500 rpm; spinning time: 30 s). A Mettler-Toledo FP900 Thermosystem was used for sample annealing.

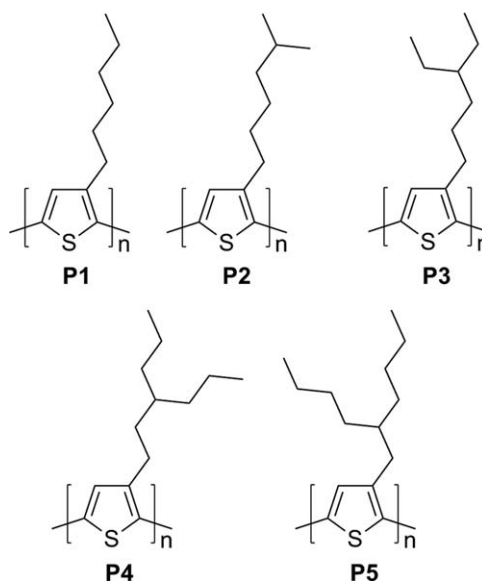


FIGURE 1 Structure of P3ATs with increasingly more bulky side chains.

2θ scans were performed on a PANalytical X'pert Pro X-ray diffractometer using Cu $K\alpha$ radiation with a wavelength of 1.54 Å. An amount of powder was placed without additional fixation on the horizontal sample holder plate with the incoming X-ray beam impinging in a fixed direction parallel to this horizontal plane while the detector was scanned.

The powders were weighted and stored under inert (argon) atmosphere.

Conventional continuous wave slow-passage X-band (~ 9.2 GHz) ESR measurements were carried out at room temperature using a Jeol FA100 spectrometer. Low microwave power ($P_{\mu} \leq 1$ mW) first derivative-absorption dP_{μ}/dB spectra were recorded through applying sinusoidal modulation (~ 100 kHz; amplitude $B_m \sim 0.35$ G) of the externally applied magnetic field B . Some of the observations were made in a locally built K -band (~ 20.6 GHz) setup, as described elsewhere.²⁸ A co-mounted calibrated MgO:Mn^{2+} reference sample was used for absolute g -factor and spin density (spin $S = 1/2$) calibration, with the latter performed through double numerical integration of the detected dP_{μ}/dB spectra. At X band, the g values of the third and fourth hyperfine-split lines of the Mn^{2+} (^{55}Mn ; 100% natural abundance; nuclear spin $I = 5/2$) sextet were calibrated as 2.0338 ± 0.0001 and 1.9807 ± 0.0001 , respectively. The attained absolute and relative accuracy is estimated at $\sim 20\%$ and $\sim 5\%$, respectively. Signal averaging (typically ~ 50 scans) was routinely applied to enhance spectral quality.

SQUID-based magnetometry is carried out in a MPMS-XL magnetometer (Quantum Design). The powders are weighted and a typical amount of 15 mg is fixed between small pieces of cotton wool inside the non-magnetic plastic transparent sample tube. The magnetic signal from the plastic sample tube with cotton wool (without the powder sample) is

measured separately. Magnetization was measured at different fixed temperatures as a function of magnetic field in RSO (reciprocating sample option) operation mode.

When measuring weak magnetic responses, one needs to be very cautious for (magnetic) contaminations.²⁹ Therefore, working conditions were kept as clean as possible and any contact of the sample powders with metals (spatula, etc.) was avoided. Moreover, control ESR experiments were performed on several samples before and after the SQUID magnetization measurements, in which no traces of known ferromagnetic metals (Fe, Co, and Ni) were detected in atomic/ionic paramagnetic form.

Compound **1c**,³⁰ **1d**,³¹ **1e**,³² and **4a**³³ were synthesized as described in literature.

Synthesis of P1–P5

General Procedure for the Synthesis of 3-Alkylthiophene

A solution of the alkyl bromide (1.1 eq) in dry diethylether (2 M) was added to a suspension of Mg (1.2 eq) in dry diethyl ether (2 M) under an argon atmosphere. After addition of the alkyl bromide, the reaction mixture was refluxed for 1 h and then allowed to cool to room temperature. Subsequently, the mixture was added to a solution of 3-bromothiophene (1 eq) and Ni(dppp)Cl₂ (0.01 eq) in dry diethyl ether (1 M) and under an argon atmosphere an refluxed overnight. After cooling to room temperature, the mixture was poured into a 1 M HCl solution and extracted with diethyl ether. The organic layer was washed with a saturated NaCl solution, dried over MgSO₄ and concentrated *in vacuo*. The crude product was further purified by column chromatography (SiO₂; eluent: petroleum ether), affording a colorless oil.

3-(5-Methylhexyl)thiophene (2b). The used reagents were **1b** (27.9 mmol; 5.00 g), 3-bromothiophene (24.3 mmol; 3.96 g), Mg (27.9 mmol; 678 mg), and Ni(dppp)Cl₂ (244 μmol; 132 mg). Yield: 1.39 g (31%). ¹H NMR (CDCl₃): δ = 7.23 (m, 1H, Ar H), 6.92 (m, 2H, Ar H), 2.62 (t, 2H, CH₂), 1.63–1.58 (m, 3H, CH₂, CH), 1.33 (m, 2H, CH₂), 1.21 (m, 2H, CH₂), 0.86 (d, 6H, CH₃). ¹³C NMR (CDCl₃): δ = 143.4, 128.4, 125.2, 119.9, 39.0, 31.0, 30.5, 28.07, 27.3, 22.8. MS: 182 (M⁺) (calc. 182.3).

3-(4-Ethylhexyl)thiophene (2c). The used reagents were **1c** (8.22 mmol; 1.59 g), 3-bromothiophene (7.50 mmol; 1.22 g), Mg (8.50 mmol; 207 mg), and Ni(dppp)Cl₂ (74.8 μmol; 40.6 mg). Yield: 707 mg (48%). ¹H NMR (CDCl₃): δ = 7.24 (m, 1H, Ar H), 6.93 (m, 2H, Ar H), 2.61 (t, 2H, CH₂), 1.62–1.57 (m, 2H, CH₂), 1.28–1.26 (m, 7H, CH₂, CH), 0.83 (t, 6H, CH₃). ¹³C NMR (CDCl₃): δ = 143.5, 128.4, 125.2, 119.89, 40.4, 32.59, 30.9, 27.9, 25.6, 11.1. MS: 196 (M⁺) (calc. 196.4).

3-(3-Propylhexyl)thiophene (2d). The used reagents were **1d** (18.9 mmol; 3.73 g), 3-bromothiophene (16.3 mmol; 2.66 g), Mg (19.6 mmol; 477 mg), and Ni(dppp)Cl₂ (88.5 μmol; 48.0 mg). Yield: 1.25 g (36%). ¹H NMR (CDCl₃): δ = 7.24

(dd, *J* = 3.1 Hz, *J* = 4.9 Hz, 1H, Ar H), 6.93 (m, 2H, Ar H), 2.61 (t, 2H, CH₂), 1.59–1.54 (m, 2H, CH₂), 1.28 (m, 9H, CH₂, CH), 0.89 (t, 6H, CH₃). ¹³C NMR (CDCl₃): δ = 143.7, 128.4, 125.2, 119.7, 36.8, 36.0, 34.62, 27.6, 19.9, 14.7. MS: 211 (MH⁺) (calc. 211.4).

3-(2-Butylhexyl)thiophene (2e). The used reagents were **1e** (10.6 mmol; 2.34 g), 3-bromothiophene (9.71 mmol; 1.58 g), Mg (11.5 mmol; 281 mg), and Ni(dppp)Cl₂ (46.1 μmol; 25.0 mg). Yield: 428 mg (20%). ¹H NMR (CDCl₃): δ = 7.22 (dd, *J* = 3.0 Hz, *J* = 4.9 Hz, 1H, Ar H), 6.90 (m, 2H, Ar H), 2.56 (d, 2H, CH₂), 1.59 (m, 1H, CH), 1.25 (m, 12H, CH₂), 0.87 (t, 6H, CH₃). ¹³C NMR (CDCl₃): δ = 142.0, 12.0, 124.9, 120.8, 39.1, 34.9, 33.2, 29.0, 23.2, 14.3. MS: 225 (MH⁺) (calc. 225.4).

General Procedure for the Bromination of the Alkylthiophenes

NBS (1 eq) was added to a solution of alkylthiophene (1 eq) in dichloromethane (0.2 M) and shielded from light. The reaction was stirred overnight under argon atmosphere. Afterwards, the reaction mixture was neutralized with a 10% Na₂S₂O₃ solution, extracted with dichloromethane, and washed with a saturated NaCl solution. The organic layer was dried with MgSO₄ and the solvent was removed under reduced pressure. The crude product was further purified with column chromatography (SiO₂; eluent: petroleum ether) to obtain a colorless oil.

2-Bromo-3-(5-methylhexyl)thiophene (3b). The used reagents were **2b** (5.00 mmol; 912 mg) and NBS (5.00 mmol; 890 mg). Yield: 1.15 g (88%). ¹H NMR (CDCl₃): δ = 7.18 (d, *J* = 5.7 Hz, 1H, Ar H), 6.79, (d, *J* = 5.7 Hz, 1H, Ar H), 2.56 (t, 2H, CH₂), 1.58–1.54 (m, 3H, CH₂, CH), 1.32 (m, 2H, CH₂), 1.21 (m, 2H, CH₂), 0.87 (d, 6H, CH₃). ¹³C NMR (CDCl₃): δ = 142.1, 128.4, 125.3, 108.9, 38.9, 30.1, 29.6, 28.1, 27.2, 22.8. MS: 262 (M⁺) (calc. 261.2).

2-Bromo-3-(4-ethylhexyl)thiophene (3c). The used reagents were **2c** (2.50 mmol; 491 mg) and NBS (2.50 mmol; 445 mg). Yield: 434 mg (63%). ¹H NMR (CDCl₃): δ = 7.18 (d, *J* = 5.6 Hz, 1H, Ar H), 6.80, (d, *J* = 5.6 Hz, 1H, Ar H), 2.54 (t, 2H, CH₂), 1.54 (m, 2H, CH₂), 1.27 (m, 7H, CH₂, CH₂), 0.83 (t, 6H, CH₃). ¹³C NMR (CDCl₃): δ = 142.1, 128.4, 125.3, 108.9, 40.3, 32.4, 29.9, 27.1, 25.5, 11.0. MS: 275 (M⁺) (calc. 275.2).

2-Bromo-3-(3-propylhexyl)thiophene (3d). The used reagents were **2d** (5.95 mmol; 1.25 g) and NBS (5.95 mmol; 1.06 g). Yield: 702 mg (41%). ¹H NMR (CDCl₃): δ = 7.18 (d, *J* = 5.6 Hz, 1H, Ar H), 6.79, (d, *J* = 5.6 Hz, 1H, Ar H), 2.54 (t, 2H, CH₂), 1.54 (m, 2H, CH₂), 1.27 (m, 9H, CH₂, CH), 0.89 (t, 6H, CH₃). ¹³C NMR (CDCl₃): δ = 142.4, 128.3, 125.3, 108.8, 36.8, 36.0, 33.7, 26.8, 19.9, 14.7. MS: 289 (MH⁺) (calc. 290.3).

2-Bromo-3-(2-butylhexyl)thiophene (3e). The used reagents were **2e** (1.91 mmol; 428 mg) and NBS (1.91 mmol; 340 mg) and the reaction mixture was heated to 40 °C. Yield: 460 mg (79%). ¹H NMR (CDCl₃): δ = 7.18 (d, *J* = 5.6 Hz, 1H, Ar H), 6.76, (d, *J* = 5.6 Hz, 1H, Ar H), 2.49 (d,

2H, CH₂), 1.64 (m, 1H, CH), 1.26 (m, 12H, CH₂), 0.88 (t, 6H, CH₃). ¹³C NMR (CDCl₃): δ = 141.3, 129.0, 125.1, 109.6, 38.7, 34.2, 33.2, 28.9, 23.2, 14.3. MS: 304 (M⁺) (calc. 303.3).

General Procedure for the Iodination of the 2-Bromo-3-alkylthiophenes

A solution of 2-bromo-3-alkylthiophene in THF (0.2 M) under argon atmosphere was shielded from light and iodine (0.5 eq) and iodobenzene diacetate (0.5 eq) were added. The reaction was stirred at room temperature for 8 h. Afterwards the reaction mixture was washed with a 10% Na₂S₂O₃ solution, extracted with Et₂O and washed with a saturated NaCl solution. The organic layer was dried with MgSO₄, the solvent and iodobenzene were removed under reduced pressure and finally, the crude product was purified with column chromatography (SiO₂; eluent: petroleum ether), affording a colorless oil.

2-Bromo-3-(5-methylhexyl)-5-iodothiophene (4b). The used reagents were **3b** (2.00 mmol; 522 mg), iodobenzene diacetate (1.00 mmol; 322 mg), and I₂ (1.00 mmol; 254 mg). Yield: 599 mg (77%). ¹H NMR (CDCl₃): δ = 6.96 (s, 1H, Ar H), 2.52 (t, 2H, CH₂), 1.54–1.52 (m, 3H, CH₂,CH), 1.31 (m, 2H, CH₂), 1.19 (m, 2H, CH₂), 0.86 (d, 6H, CH₃). ¹³C NMR (CDCl₃): δ = 144.4, 138.1, 111.8, 71.2, 38.8, 30.1, 29.4, 28.0, 27.1, 22.8. MS: 388 (M⁺) (calc. 387.1).

2-Bromo-3-(4-ethylhexyl)-5-iodothiophene (4c). The used reagents were **3c** (1.25 mmol; 344 mg), iodobenzene diacetate (625 μmol; 201 mg), and I₂ (625 μmol; 159 mg). Yield: 439 mg (88%). ¹H NMR (CDCl₃): δ = 6.97 (s, 1H, Ar H), 2.50 (m, 2H, CH₂), 1.52 (m, 2H, CH₂), 1.27 (m, 7H,CH₂, CH), 0.83 (t, 6H, CH₃). ¹³C NMR (CDCl₃): δ = 144.5, 138.1, 111.8, 71.1, 40.3, 32.4, 29.7, 27.0, 25.5, 11.0. MS: 402 (M⁺) (calc. 401.1).

2-Bromo-3-(3-propylhexyl)-5-iodothiophene (4d). The used reagents were **3d** (2.00 mmol; 579 mg), iodobenzene diacetate (1.00 mmol; 322 mg), and I₂ (1.00 mmol; 254 mg). Yield: 789 mg (95%). ¹H NMR (CDCl₃): δ = 6.96 (s, 1H, Ar H), 2.50 (t, 2H, CH₂), 1.49–1.43 (m, 2H, CH₂), 1.30–1.26 (m, 9H, CH₂, CH), 0.89 (t, 6H, CH₃). ¹³C NMR (CDCl₃): δ = 144.7, 138.1, 111.6, 71.2, 36.8, 35.9, 33.6, 26.7, 19.9, 14.6. MS: 416 (MH⁺) (calc. 416.2).

2-Bromo-3-(2-butylhexyl)-5-iodothiophene (4e). The used reagents were **3e** (1.52 mmol; 460 mg), iodobenzene diacetate (0.76 μmol; 245 mg), and I₂ (0.76 μmol; 193 mg). Yield: 436 mg (67%). ¹H NMR (CDCl₃): δ = 6.92 (s, 1H, Ar H), 2.66 (d, 2H, CH₂), 1.60–1.54 (m, 1H, CH), 1.26 (m, 12H, CH₂), 0.88 (t, 6H, CH₃). ¹³C NMR (CDCl₃): δ = 143.7, 138.6, 112.5, 71.1, 38.7, 34.0, 33.1, 28.9, 23.2, 14.3. MS: 430 (MH⁺) (calc. 430.2).

General Procedure for the Polymerization of the Poly(3-alkylthiophene)s

To a solution of 2-bromo-3-alkyl-5-iodothiophenes (1 eq) in dry THF (0.1 M) was added 1 eq of *i*-PrMgCl·LiCl at room temperature and under an argon atmosphere. The solution was further stirred for 1 h and subsequently added to a

suspension of Ni(dppp)Cl₂ (2.5 mol %) in dry THF under an argon atmosphere. After stirring the solution overnight at room temperature, the reaction mixture was quenched with a 1 M HCl solution and precipitated in MeOH. The filtrate was further extracted with MeOH and CHCl₃ (**P1–P3**, **P5**) or chlorobenzene (**P4**). The CHCl₃ (or chlorobenzene) soluble fraction was precipitated in MeOH, filtered off, and dried.

Synthesis of P1. The used reagents were **4a** (1.00 mmol; 373 mg), *i*-PrMgCl·LiCl (1.10 M in THF; 1.00 mmol; 910 μL), and Ni(dppp)Cl₂ (25.0 μmol, 13.6 mg). Yield CHCl₃ fraction: 126 mg (76%).

Synthesis of P2. The used reagents were **4b** (1.00 mmol; 387 mg), *i*-PrMgCl·LiCl (1.10 M in THF; 1.00 mmol; 910 μL), and Ni(dppp)Cl₂ (25.0 μmol, 13.6 mg). Yield CHCl₃ fraction: 128 mg (71%).

Synthesis of P3. The used reagents were **4c** (675 μmol; 271 mg), *i*-PrMgCl·LiCl (1.10 M in THF; 675 μmol; 615 μL), and Ni(dppp)Cl₂ (16.9 μmol, 9.10 mg). Yield CHCl₃ fraction: 90.5 mg (69%).

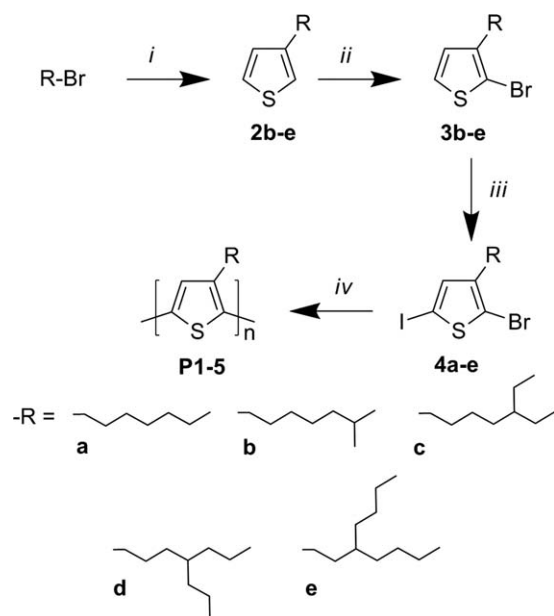
Synthesis of P4. The used reagents were **4d** (716 μmol; 297 mg), *i*-PrMgCl·LiCl (1.10 M in THF; 716 μmol; 651 μL), and Ni(dppp)Cl₂ (17.9 mmol, 9.70 mg). Yield chlorobenzene fraction: 118 mg (79%).

Synthesis of P5. The used reagents were **4e** (1.20 mmol; 516 mg), *i*-PrMgCl·LiCl (1.10 M in THF; 1.20 mmol; 1.10 mL), and Ni(dppp)Cl₂ (30.0 μmol, 16.3 mg). Yield CHCl₃ fraction: 216 mg (81%).

RESULTS AND DISCUSSION

Polymer Synthesis

The polymers were prepared by the Ni(dppp)-mediated polymerization (dppp = 1,3-diphenylphosphinopropane) of P3ATs to yield regio-regular polymers.^{27,33} The synthesis of the monomers starts with a Kumada-coupling of the respective alkyl Grignard reagents **1b–e**, prepared *in situ* from the corresponding bromides, and 3-bromothiophene (Scheme 1). In the next step, 3-alkylthiophene **2b–e** is brominated with NBS in the 2-position, followed by an iodination at the 5-position with iodine and iodobenzene diacetate resulting in **4a–e**. The polymerization of **P1–P5** starts with the *in situ* GRIM metathesis of **4a–e** with *i*-PrMgCl·LiCl as Grignard reagent, followed by a polymerization with Ni(dppp)Cl₂ (2.5 mol %) as catalyst to yield **P1–P5**. The use of *i*-PrMgCl·LiCl and not *i*-PrMgCl as Grignard reagent is motivated by the fact that we found that the former resulted in a lower degree of polymerization and lower yields for the more sterically hindered monomers (**4d** and **4e**). Indeed, Wu et al.³⁴ and Lamps et al.³⁵ found that LiCl increases the reactivity of the monomers in such way that HH couplings, which are not formed in the absence of LiCl for steric reasons, become possible using Ni(dppp) as catalytic moiety. Applied on our monomers, we speculated that the presence of LiCl would also tackle a possible slower polymerization of alkylthiophenes



SCHEME 1 Synthesis of the monomers and polymers P1–P5. Conditions: (i) (1) Mg, (2) Ni(dppp)Cl₂, 3-bromothiophene, (ii) NBS, (iii) I₂, PhI(OAc)₂, (iv) (1) *i*-PrMgCl-LiCl, (2) Ni(dppp)Cl₂.

with a bulky substituent, as in **P5**, which turned out to be the case. After polymerization, the crude polymer was precipitated in methanol, isolated and further purified via Soxhlet extractions with methanol and chloroform. The chloroform fraction was concentrated, precipitated in methanol and dried *in vacuo*.

During its synthesis, **P4** showed an anomalous behavior as it visually precipitated during the polymerization and only (slightly) dissolved in (warm) chlorobenzene. The synthesis of **P4** was repeated twice, but the same result was obtained. Due to its deviant behavior and its rather insolubility, **P4** was not withdrawn for further study.

The structure of **P1–P3**, **P5** was confirmed by ¹H NMR (Supporting Information Fig. S25–S29) and the degree of polymerization was also calculated by relative integration of the inner and terminal methylene protons (Table 1). The number averaged molar mass (\overline{M}_n) and polydispersity (*D*) of the polymers **P1–P5** were also determined by GPC in THF toward polystyrene standards (Table 1).

DSC and XRD Analysis

Next, the polymers were subjected to DSC analysis. Typically the second heating scan was used. Initially, no melting was observed for **P5**, pointing at the fact that **P5** is amorphous after a relative fast cooling (20 K/min). However, Boudouris et al.³⁶ have shown for HT-coupled poly(3-(2-ethylhexyl)thiophene), which also has a relative bulky, branched side-chain, that the polymer is actually not amorphous, but that it slowly crystallizes. Since the magnetic measurements are performed on powders which were allowed to stand at room temperature for a long time, the DSC experiments were repeated after three days of standing. We opted for this

TABLE 1 Molar mass and DSC data of **P1–P5**

P3ATs	\overline{M}_n^a (kg/mol)	<i>D</i> ^a	DP ^b	<i>T</i> _m (°C)	ΔH (J/g)
P1	6.2	1.1	23	201	18.1
P2	8.7	1.4	29	197	17.3
P3	8.0	1.4	23	159	16.4
P4	8.4	1.1	26	65	11.9

^a Determined by GPC in THF towards poly(styrene) standards.

^b Relative integration of the inner and terminal methylene ¹H NMR resonances.

“thermal treatment” and not for, for example, a conventional annealing, since this former treatment better reflects the actual history of the samples prior to the magnetic measurements. This revealed that in all samples except **P1** ΔH increases after standing for 3 days and that **P5** showed a clear melting peak. If the *T*_m and ΔH are considered for all polymers, it is clear that the more the side-chain is branched, the lower *T*_m and ΔH become. This already suggests that the π -interactions, a driving force for the crystallization, weaken as more bulky substituents are used. It is also in line with the behavior of poly(3-(2-ethylhexyl)thiophene): the bulkiness of the side-chains does not necessarily impede the crystallization, it only slows down its speed and reduces *T*_m and ΔH .

The crystalline nature of all samples, including **P5**, was confirmed by X-ray diffraction. The measurements were performed on samples that were stored at room temperature for many days, which allows crystallization. Figure 2 shows the X-ray intensity versus 2 θ traces for **P1–P3** and **P5**.

The (100) peak reflects the distance between the planes containing the stacked polythiophene backbones. For **P1** with the least bulky side chains, this distance is found to

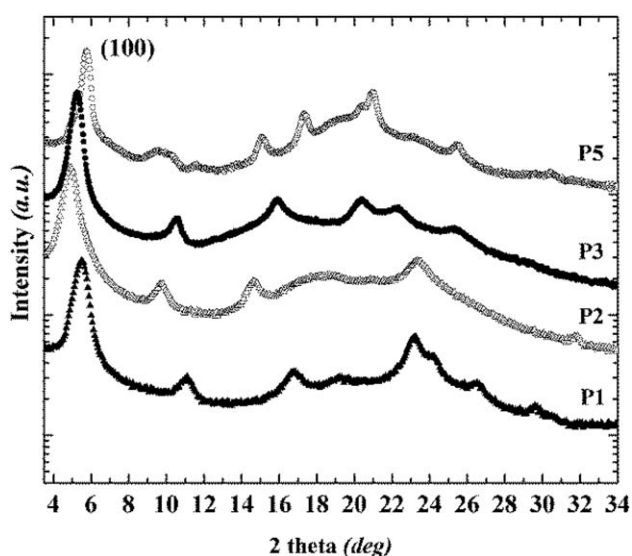


FIGURE 2 XRD spectra of **P1–P3**, **P5**. The curves are vertically shifted for clarity.

be $16.07 \pm 0.02 \text{ \AA}$. It is clear from Figure 2 that the distance along the (100) direction between the stacked polythiophene backbone planes changes when the side chains become more bulky in **P2**, **P3**, and **P5**. For **P2**, the inter-backbone distance increases to $18.05 \pm 0.02 \text{ \AA}$. For **P3** and **P5**, we notice however an opposite trend with the distance reducing to $16.82 \pm 0.02 \text{ \AA}$ and $15.35 \pm 0.02 \text{ \AA}$, respectively. This strongly suggests that there is a transition from a quasi-orthorhombic unit cell to a monoclinic (or triclinic) one, in which the thiophene monomers of neighboring backbones are slightly shifted with respect to each other instead of orthogonally opposite. Such a tilted unit cell would indeed create more space to accommodate for the bulky side chains even if it reduces the distance between neighboring planes of stacked backbones. Based on the shifted (100) reflections, we can obtain a lower limit for the monoclinic angle of the tilted unit cell (i.e., the angle between the plane of the stacked polymer chains and the plane containing the side chains). Herefore, we reasonably assume that the distance between the polythiophene backbones in the plane containing the side chains will not decrease with increasing bulkiness of the side chains in **P3** and **P5**. For **P5**, we find a lower limit for the deviation/tilt of $17.2 \pm 0.4^\circ$ with respect to the 90° orthorhombic angle.

This is in line with the findings of Boudouris et al.,³⁶ who demonstrated a large discrepancy of 90° and a triclinic unit cell for the branched poly(3-(2-ethylhexyl)thiophene). As a consequence, it was unfortunately not possible to determine all unit cell parameters using XRD.

Optical Characterization

The optical behavior of **P1–P3** and **P5** was investigated both in good solvent, upon addition of non-solvent and in film. In good solvent, such as chloroform, the λ_{max} of all polymers is more or less equal; only **P5**, which has the most bulky side chain, shows a slight blue shift in chloroform, meaning that the increased bulkiness of the substituent of **P5** results in a more twisted conformation around the consecutive thiophene moieties [Fig. 3(A)]. Next, UV-vis spectra of **P1–P3** and **P5**, with approximately the same concentration, were recorded in different ratios of $\text{CHCl}_3/\text{MeOH}$ (Supporting Information Fig. S30). Upon increasing the amount of methanol, all polymers except **P5** aggregate, as is evidenced by a large red-shift and formation of fine structure. **P5** shows only a minor red-shift, which demonstrates that in this condition, it planarizes to some extent, but does not stack. Clearly, the stacking in **P5** is prohibited by the bulky side chains. The difference between **P1–P3** is that the aggregation starts at higher non-solvent concentration for the polymers with more bulky side chains and that there is also a decrease in fine structure in aggregated state upon increasing the bulkiness of the side chains [Fig. 3(B)]. As mentioned previously,^{25,26} the absorption spectrum of aggregated P3AT consists of three chromophores. One band [Fig. 3(C)] is related to the polymer in its disordered, random coil like conformation (around 450 nm). The second transition comes from the individual, planar, and stacked polymer chains

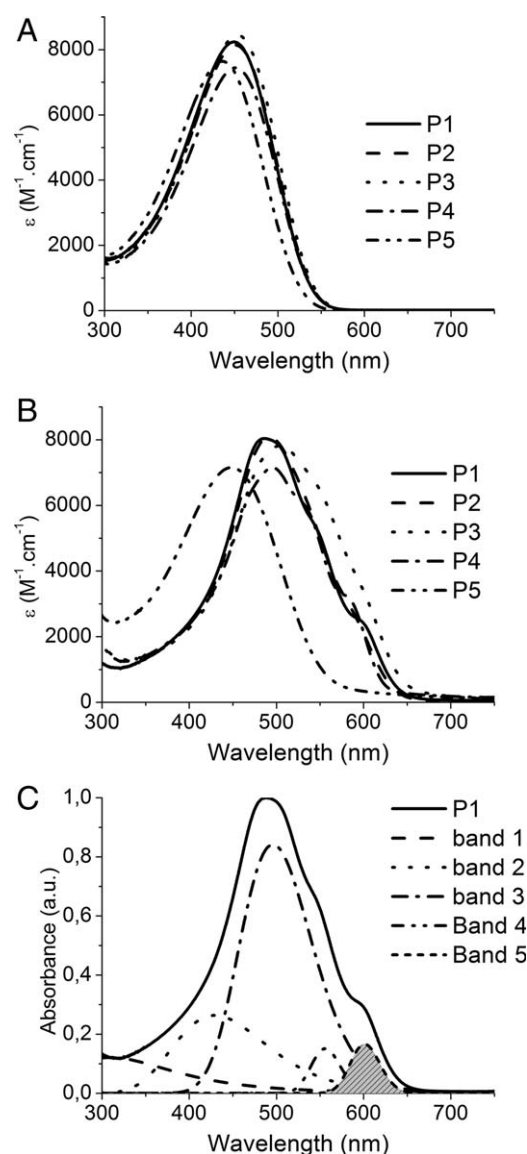


FIGURE 3 (A) UV-vis spectra of **P1–P3**, **P5** in chloroform; $c_{\text{P1}} = 1.69 \times 10^{-4} \text{ M}$; $c_{\text{P2}} = 1.71 \times 10^{-4} \text{ M}$; $c_{\text{P3}} = 1.73 \times 10^{-4} \text{ M}$; $c_{\text{P4}} = 1.55 \times 10^{-4} \text{ M}$; $c_{\text{P5}} = 1.82 \times 10^{-4} \text{ M}$; (B) UV-vis spectra of **P1–P5** in non-solvent; **P1–P3**, **P5** $\text{CHCl}_3/\text{MeOH}$ (10/90); $c_{\text{P1}} = 1.69 \times 10^{-4} \text{ M}$; $c_{\text{P2}} = 1.71 \times 10^{-4} \text{ M}$; $c_{\text{P3}} = 1.73 \times 10^{-4} \text{ M}$; $c_{\text{P5}} = 1.82 \times 10^{-4} \text{ M}$. (C) Deconvolution of the spectrum of **P1** in $\text{CHCl}_3/\text{MeOH}$ (10/90).

(around 530 nm, with vibronic fine-structure). The last transition arises from a transition dipole moment, delocalized over multiple, aggregated polymer chains (around 610 nm for P3AT). The absorption spectra of **P5** essentially consist of only one band of coiled polymer chains. Deconvolution of the UV-vis spectra in poor solvent using a linear programming method [Fig. 3(C) for **P1** and Supporting Information Fig. S31 for **P2**, **P3**, and **P5**] reveals the different bands discussed above: band 2 corresponds to the polymer in its random coil like conformation, band 3 and 4 to the individual, planar, stacked polymer chains with exciton coupling and band 5 to a transition dipole moment, which is delocalized

TABLE 2 Relative intensity of the different “chromophores” of the polymers in the aggregated state

	In poor solvent		In film	
	Band 3 + 4%	Band 5%	Band 3 + 4%	Band 5%
P3ATs				
P1	61.9	4.4	72.5	5.4
P2	61.7	3.8	63.5	4.4
P3	64.2	2.6	77.4	2.6
P5	30.4	0	54.6	1.4

over multiple polymer chains and which therefore depends on the π -interactions. The relative contribution of planar polymer chains (sum of bands 3 + 4) and of the band due to π -interactions (band 5) is shown in Table 2. Looking at the low energy band (band 5), it is clear that upon increasing the bulkiness of the side chain, a decrease in intensity of the low energy band is observed, pointing at smaller π -interactions. The amount of planar stacked chains in **P5** is considerably less than this for the other polymers, which indicates that in **P5**, the planarization of the polymer chains is more difficult due to its bulky side chains. Surprisingly, the amount of planar polymer chains is the highest in **P3**.

Also fluorescence spectroscopy was carried out in good (CHCl_3) as well as in poor solvent $\text{CHCl}_3/\text{MeOH}$ [1/9]). **P1–P3** were excited at 440 nm and **P5** was excited at 425 nm. From Supporting Information Figure S32, it is clear that always the same emission is found in good solvent. Thus, the emitting chromophore is essentially the same for **P1–P5**, which means that all the polymers adopt the same random coil like structure in good solvent. In non-solvent, in contrast (Supporting Information Fig. S33), the bulkiness of the side chain clearly influences the quenching of the emission. Upon increasing the bulkiness, going from **P1** to **P3**, which increases the distance between the polymer chains, aggregation becomes less pronounced and the quenching of the fluorescence is less efficient. This is expressed in an increase in intensity of the signal, which originates from residual coiled polymer chains. **P5**, which does not aggregate in non-solvent, has a λ_{em} at higher wavelength, which indicates that another, more planar chromophore is present in non-solvent that weakly emits at higher wavelength.

Next, the experiments were repeated on spin coated films of **P1–P3** and **P5**. First, it was verified whether the polymers are not trapped in a (partly) amorphous structure, as was the case when the polymers were melted and cooled down relatively fast (see “DSC and XRD analysis” section). Annealing did not affect the spectra of **P1–P3**; the UV-vis spectrum of **P5**, however, changed dramatically. Clearly, melting the polymer and subsequently cooling it down traps the polymer in its amorphous, coiled configuration, as shown by its UV-vis spectrum and which is fully in line with the DSC measurements. Next, we monitored the crystallization of the polymer at room temperature by recording UV-vis spectra at different times. From Figure

4(B), it is clear that **P5** does crystallize, which is in line with the DSC results but different from the situation in poor solvent and that the crystallization in thin films takes 30–45 min.

Next, the spectra of the polymers were deconvoluted (Supporting Information Fig. S34). The relative ratio of band 3 + 4, pointing at planar polymer chains and of band 5, indicating π -stacking, is shown in Table 2. First, it is clear that π -interactions are present in all polymers, also in **P5**, but that increasing the bulkiness results in smaller π -interactions. Second, the highest fraction of planar polymer chains is also in film found for **P3**, followed by **P1**.

ESR Spectroscopy

The magnetic behavior of the polymers was first studied by X-band ESR spectroscopy at 300 K (Fig. 5 for **P1** and in Supporting Information Fig. S35 for **P2–P5**). Prior to measurement, the powder samples were treated with an alcoholic hydrazine solution and dried under argon to avoid polaron formation by oxidation in ambient air. As illustrated in Figure 5, only one signal, of symmetric shape, is observed with g value in the range 2.0030–2.0045. The (inferred) spin densities, g -values, and line widths and shapes are listed in Table 3. Depending on the degree of supramolecular order, the line shape of an ESR signal varies from Gaussian to

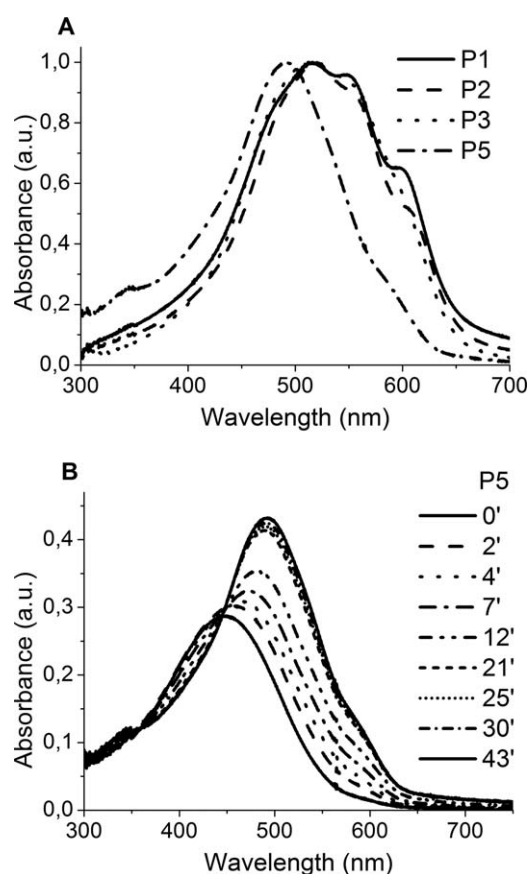


FIGURE 4 (A) UV-vis spectra (normalized) of the polymers after annealing; (B) UV-vis spectra of **P5** in function of time after melting and fast cooling.

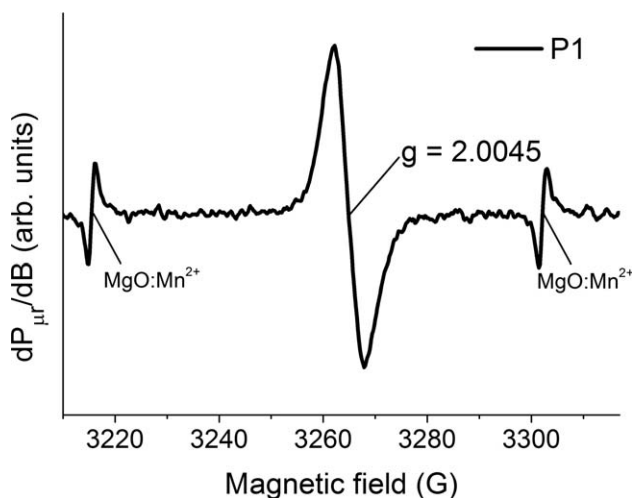


FIGURE 5 X-band (~ 9.2 GHz) first-derivative absorption spectrum measured on **P1** at room temperature using $P_{\mu} = 0.5$ mW and $B_m = 0.35$ G.

Lorentzian. A signal with a Lorentzian line shape is generally an indication of homogeneous broadening as met when the ESR-active centers are embedded in an environment of high degree of order. This conclusion is supported by the smaller line width of the signal from **P1**. An increase in line width (ΔB_{pp}) accompanied by a change in line shape from Lorentzian over Voigt to, finally, Gaussian points to gradually more disorder being introduced into the system (e.g., g -spread broadening). As such, the line shape provides crucial information on the order present in the environment of the electron spins. The ESR data thus clearly confirm that increasing the bulkiness of the side chain leads to a decrease in the supramolecular order of the polymer samples, which is in perfect agreement with the results obtained from the UV-vis and DSC measurements.

Looking at the number of spin centers for **P1–P5**, it is clear that for all the samples the densities have the same order of magnitude in agreement with previously obtained results for P3ATs in the neutral state.²⁵ The g values for **P2–P5** are equal within experimental accuracies, only for **P1** a small increase in g value is observed compared to the other polymers studied here. It may indicate the signal to originate from a spin system that is more localized than for the other samples. For reasons of completeness, it should be added

TABLE 3 ESR spin densities ($S = 1/2$), g -value, and line widths (ΔB_{pp}) observed on **P1–P3**, **P5** P3AT materials

P3ATs	Spin density ($\times 10^{16} \text{ g}^{-1}$)	g value (1×10^{-4})	ΔB_{pp} (G)	Line shape
P1	4.0 ± 0.1	2.0045	4.8 ± 0.1	Lorentzian
P2	8.0 ± 0.1	2.0031	5.9 ± 0.4	Voigt
P3	1.5 ± 0.1	2.0032	6.6 ± 0.2	Voigt
P5	1.3 ± 0.1	2.0030	10.4 ± 0.2	Gaussian

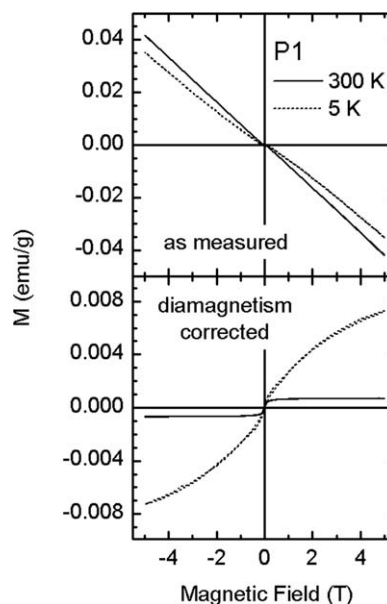


FIGURE 6 $M(H)$ data of **P1**. *Top*: as measured. *Bottom*: after subtraction of the diamagnetic component.

that an additional spin system is observed in sample **P3**, showing an angle dependent ESR signal of Lorentzian line shape at $g = 2.44$ (Supporting Information Fig. S36). But recalling that the ESR experiments are carried out on powder samples, the observed angle dependence of the signal is to be ascribed to the overall shape of the ESR sample being not a perfect cylinder (demagnetization effects related to distinct magnetic properties).

In summary, the ESR results confirm the supramolecular behavior observed by UV-vis spectroscopy and DSC. The data are also in line with our previous results obtained on polythiophenes.

SQUID Magnetometry

The magnetic properties of the polymers were next measured by SQUID magnetometry on the same powders as for the ESR measurements. By comparing the magnetization measurements performed *with* and *without* the polymer sample (the latter corresponding to the contribution of the sample holder, i.e., the plastic tube and the cotton), six different components can be identified: diamagnetic-, paramagnetic-, and ferromagnetic-like components originating from the sample holder; diamagnetic-, paramagnetic-, and ferromagnetic-like components of the polymer sample. The two diamagnetic components correspond to the expected diamagnetic behavior of the materials in question. Although these diamagnetic components dominate the measured magnetization, since they are (to a good approximation) linear in applied magnetic field and temperature-independent, they can be easily separated from the paramagnetic and ferromagnetic-like components. Figure 6 shows the magnetization of sample **P1** before and after subtraction of the diamagnetic component. The diamagnetism-corrected data is

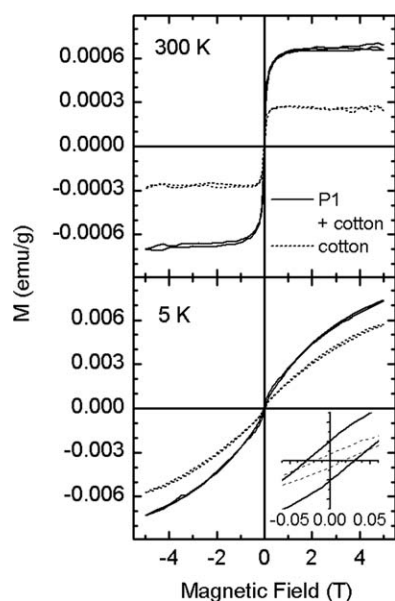


FIGURE 7 $M(H)$ data of **P1**, compared to the background from the sample holder (mostly due to the cotton enclosing the polymer).

given by $M - \chi H$, where H is the magnetic field and χ is the diamagnetic susceptibility $\Delta M/\Delta H$ estimated at 300 K in the high field (4–5 T) region. The paramagnetic component observed in the sample holder can be ascribed to paramagnetic contaminants present in the cotton (e.g., paramagnetic metallic compounds or dilute transition-metal ions). Similarly, the ferromagnetic-like component observed in the sample holder can be ascribed to ferromagnetic contaminants in the cotton (e.g., ferromagnetic Fe-containing compounds, such as metallic Fe and Fe oxides). The magnetization (paramagnetic- and ferromagnetic-like components) originating from the polymer samples can be inferred from comparing the diamagnetism-corrected magnetization measured *with* and *without* the polymer sample—direct subtraction has not been performed since it introduces significant artifacts in the magnetization curve, especially at the low field (low magnetization) region of interest. The paramagnetic component of the polymer samples is associated with the spin centers identified in the ESR measurements. Figure 7 shows such a comparison for sample **P1**. In fact, the paramagnetic component is only visible at 5 K. At 300 K, the (Brillouin-like) magnetization is, to a good approximation, linear in applied magnetic field (and orders of magnitude smaller compared to that at 5 K), and is therefore also subtracted when subtracting the diamagnetic component. Consequently, the corrected magnetization, at 300 K, corresponds to the ferromagnetic-like component. At 5 K, both the paramagnetic- and ferromagnetic-like components are visible, although the former dominates the magnetization. In general, at room temperature, all polymers show ferromagnetic-like behavior with negligible coercivity. At 5 K, only **P1** shows a coercivity value (350 Oe) which is significantly higher than that of cotton (150 Oe). For the other polymers, the 5 K

coercivity values are comparable to those of the cotton sample holder, and therefore cannot be reliably determined.

Before analyzing, in detail, the observed magnetic properties, it is important to note that the ferromagnetic moments detected in these polymers is very small (of the order 3×10^{-4} emu/g, i.e., 3×10^{-6} emu for a typical 10 mg sample). This is, however, a regime where magnetic contamination may play an important role. A moment of 3×10^{-6} emu corresponds, for example, to about 0.02 μg (i.e., about 2 ppm) of metallic Fe. This means that the observed magnetic properties may originate, at least partially, from accidental sample contamination with a few dust particles (typically containing ferromagnetic Fe-containing compounds), for example, during sample manipulation (cf. related discussion in Ref. 29). Staying below such contamination levels is extremely challenging, requiring that all sample preparation and characterization is carried out under clean-room conditions. Sample characterization with respect to such contaminants is also extremely challenging for several reasons: the contaminant material is not necessarily uniformly distributed in the sample, making any quantitative assessment very difficult; the number of contaminating particles may easily increase or decrease between different characterization steps, making it almost impossible to directly compare quantitative data from different techniques (e.g., magnetization vs. amount of contaminant); even if the amount of potentially magnetic elements (e.g., Fe, Co, etc.) could be precisely and reproducibly determined, it is nearly impossible to determine what fraction of these elements is in a ferromagnetic phase (e.g., ferromagnetic vs. non-ferromagnetic compounds). Therefore, although the trends observed here (discussed below) and in our previous work support an intrinsic origin, we cannot completely exclude that the observed ferromagnetism originates from magnetic contamination. In the following discussion, we assume that the observed ferromagnetism is an intrinsic property of the synthesized polymers.

As already indicated in the introduction, we hypothesize that the saturation magnetization correlates with the number of planar polymer chains, while the coercivity is influenced by π -interactions. Both entities—the number of planar polymer chains and the π -interactions—can be quantified from the UV-vis spectra. The results of the films that were kept for 1 h at room temperature were used for this evaluation, since this resembles best the powders used for the SQUID measurements. If the coercivity is considered, only **P1** shows a value (350 Oe) that is significantly higher than that of cotton (150 Oe). Because **P1** also shows the highest integration of the band related with π -interactions, this finding is in line with our hypothesis. Unfortunately, since the low temperature coercivity of the other polymers could not be determined with sufficient accuracy because it is of the same order as the small coercivity of the cotton sample, the other polymers cannot be used to further validate our hypothesis. This requires polymers with stronger π -interactions than **P1**, rather than weaker. Further

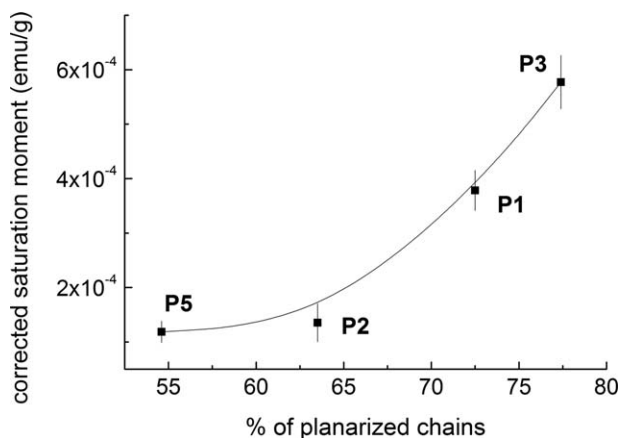


FIGURE 8 Plot of the saturation magnetization at room temperature and the integration of the bands related to planar polymer chains [band 3 and 4, Fig. 2(C)]. The curve is added as a guide for the eye.

research in this respect is underway. In order to evaluate the influence of the fraction of planar polymer chains on the saturation magnetization, the relative integration of the absorption bands 3 and 4 was plotted versus the saturation magnetization (Fig. 8). Interestingly, the surprisingly higher value for the integration of absorption bands 3 + 4 of **P3** compared to **P1** and **P2** is also reflected in the magnetization data. In general, it is observed that samples with larger fractions of planarized chains also reveal larger values of their saturation magnetization. Therefore, the SQUID results are in line with our hypotheses on the magnetic properties of neutral conjugated polymers.

CONCLUSIONS

In conclusion, a series of regio-regular P3ATs with an increasing degree of bulkiness of the alkyl side chain has been successfully synthesized with Ni(dppp)Cl₂ as a catalyst. UV-Vis spectroscopy was used to study the supramolecular aggregation of the polymer both in poor solvent and in film. In particular, deconvolution of the spectra allowed to “quantify” the π -interactions and planarization of the polymer chains. It was shown that as the bulkiness of the polymers’ side chain increases, the π -interactions and planarization diminishes. In poor solvent, the polymer with the most bulky substituent does not aggregate, while in film, this polymer does stack, showing a band originating from π -interactions, but the aggregate formation takes 30–45 min to occur. This delayed aggregation was confirmed by DSC measurements; XRD measurements confirmed that powders of all polymers are semi-crystalline. ESR measurements, performed on powder samples at 300 K, revealed a steady increase in line width and change in shape of the singly observed signal as the polymers’ substituent becomes more bulky, which denotes an increase in disorder. Thus, the ESR data reflect the same trend as previously found from the optical data. The analysis of the magnetometry data, measured at 5 and 300 K, are in line with our previously established hypotheses.

ACKNOWLEDGMENTS

We are grateful to the Onderzoeksfonds KU Leuven/Research Fund KU Leuven, the Flemish Concerted Action (GOA), the Belgian Interuniversity Poles of Attraction (IAP, FWO-Vlaanderen) and the Air Force Office of Scientific Research.

REFERENCES AND NOTES

- 1 A. Skotheim, J. Reynolds, Eds.; Handbook of Conducting Polymers, 3rd ed., CRC Press: Boca Raton, FL, **2007**.
- 2 J. L. Bredas, G.B. Street, *Acc. Chem. Res.* **1985**, *18*, 309–315.
- 3 A. J. Fisher, W. Hayes, D. S. Wallace, *J Phys: Condens Matter* **1989**, *1*, 5567–5593.
- 4 T. Ikoma, S. Okada, H. Nakanishi, K. Akiyama, S. Tero-Kubota, K. Möbius, S. Weber, *Phys. Rev. B* **2002**, *66*, 014423.
- 5 A. A. Ovchinnikov, *Theor Chim Acta* **1978**, *47*, 297–304.
- 6 W. T. Borden, E. R. Davidson, *J. Am. Chem. Soc.* **1977**, *99*, 4587–4594.
- 7 G. Kothe, K.-H. Denkel, W. Sümmermann, *Angew. Chem. Int. Ed.* **1970**, *9*, 906–907.
- 8 A. Rajca, S. Rajca, *J Chem Soc: Perkin Trans* **1998**, *2*, 1077–1082.
- 9 H. Tomioka, M. Hattori, K. Hirai, K. Sato, D. Shiomi, T. Takui, K. Itoh, *J. Am. Chem. Soc.* **1998**, *120*, 1106–1107.
- 10 H. Murata, D. Miyajima, H. Nishide, *Macromolecules* **2006**, *39*, 6331–6335.
- 11 H. Nishide, T. Maeda, K. Oyaizu, E. Tsuchida, *J. Org. Chem.* **1999**, *64*, 7129–7134.
- 12 T. Kaneko, T. Makino, H. Miyaji, M. Teraguchi, T. Aoki, M. Miyasaka, H. Nishide, *J. Am. Chem. Soc.* **2003**, *125*, 3554–3557.
- 13 A. Rajca, S. Rajca, J. Wongsriratanakul, *J. Am. Chem. Soc.* **1999**, *121*, 6308–6309.
- 14 P. K. Kahol, A. Raghunathan, B. J. McCormick, *Synth. Met.* **2004**, *140*, 261–267.
- 15 P. Dallas, D. Stamopoulos, N. Boukos, V. Tzitzios, D. Niarchos, D. Petridis, *Polymer* **2007**, *48*, 3162–3169.
- 16 N. A. Zaidi, S. R. Giblin, I. Terry, A.P. Monkman, *Polymer* **2004**, *45*, 5683–5689.
- 17 Y. Long, Z. Chen, J. Shen, Z. Zhang, L. Zhang, H. Xiao, M. Wan, J. L. Duvail, *J. Phys. Chem. B* **2006**, *110*, 23228–23233.
- 18 K. Mizoguchi, N. Kachi, H. Sakamoto, K. Kume, K. Yoshioka, S. Masubuchi, S. Kazama, *Synth. Met.* **1997**, *84*, 695–698.
- 19 A. Konkin, H.-K. Roth, P. Scharff, A. Aganov, O. Ambacher, S. Sensfuss, *Solid State Commun* **2009**, *149*, 893–897.
- 20 H. Nalwa, *Phys. Rev. B* **1989**, *39*, 5964–5974.
- 21 K. Sugiyama, T. Kojima, H. Fukuda, H. Yashiro, T. Matsuura, Y. Shimoyama, *Thin Solid Films* **2008**, *516*, 2691–2694.
- 22 F. R. de Paula, L. Walmsley, E. C. Pereira, A. J. A. de Oliveira, *J Magn Magn Mater* **2008**, *320*, e193–e195.
- 23 O. R. Nascimento, A. J. A. de Oliveira, E. C. Pereira, A. A. Correa, L. Walmsley, *J Phys: Condens Matter* **2008**, *20*, 035214.
- 24 M. Nechtschein, F. Devreux, F. Genoud, M. Guglielmi, K. Holczer, *Phys. Rev. B* **1983**, *27*, 61–78.
- 25 S. Vandeleene, M. Jivanescu, A. Stesmans, J. Cuppens, M. J. Van Bael, H. Yamada, N. Sato, T. Verbiest, G. Koeckelberghs, *Macromolecules* **2010**, *43*, 2910–2915.
- 26 S. Vandeleene, M. Jivanescu, A. Stesmans, J. Cuppens, M. J. Van Bael, T. Verbiest, G. Koeckelberghs, *Macromolecules* **2011**, *44*, 4911–4919.

- 27** E. E. Sheina, J. Liu, M. C. Iovu, D. W. Laird, R. D. McCullough, *Macromolecules* **2004**, *37*, 3526–3528.
- 28** A. Yokoyama, R. Miyakoshi, T. Yokozawa, *Macromolecules* **2004**, *37*, 1169–1171.
- 29** L. M. C. Pereira, J. P. Araújo, M. J. Van Bael, K. Temst, A. Vantomme, *J Phys D: Appl Phys* **2011**, *44*, 215001.
- 30** F. S. Prout, J. Cason, *J. Org. Chem.* **1949**, *14*, 132–136.
- 31** J. Malthête, J. Canceill, J. Gabard, J. Jacques, *Tetrahedron* **1981**, *37*, 2823–2828.
- 32** B. J. Meakin, F. R. Mumford, E.R. Ward, *J Pharm Pharmacol* **1959**, *11*, 540–547.
- 33** R. Miyakoshi, A. Yokoyama, T. Yokozawa, *J. Am. Chem. Soc.* **2005**, *127*, 17542–17547.
- 34** S. Wu, L. Huang, H. Tian, Y. Geng, F. Wang, *Macromolecules* **2011**, *44*, 7558–7567.
- 35** J.-P. Lamps, J.-M. Catala, *Macromolecules* **2011**, *44*, 7962–7968.
- 36** B. W. Boudouris, V. Ho, L. H. Jimison, M. F. Toney, A. Salleo, R. A. Segalman, *Macromolecules* **2011**, *44*, 6653–6658.